IEEE Access
Multidisciplinary ⋮ Rapid Review ⋮ Open Access Journal

Received November 18, 2020, accepted November 30, 2020, date of publication December 4, 2020,
date of current version December 17, 2020.

Digital Object Identifier 10.1109/ACCESS.2020.3042531

Phase Random Metasurface With Diffuse Scattering Based on Subwavelength Unit's Design of Shunt Resonance Circuit

ZHAOBIN CHEN[1], HUI DENG[1], AND LI ZHENG[2]
[1]School of Electronics and Information Engineering, Beihang University, Beijing 100191, China
[2]Beijing Electro-mechanical Engineering Institute, Beijing 100074, China

Corresponding author: Hui Deng (dh19@buaa.edu.cn)

ABSTRACT It is known that metasurface composed of randomly distributed subwavelength unit cells with different reflection phases features some specific electromagnetic behaviors, of which diffuse scattering property can be applied to reduce Radar Cross Section (RCS). In this paper, a subwavelength unit cell based on shunt resonance is designed. Since shunt resonance can provide stable phase distribution within the range between its double resonant frequency points, reflection phase variation of the subwavelength unit cell can be slight. Equivalent transmission line model presented proves effective on extracting reflection phase of a sub-wavelength unit cell. Referring to variation of its normalized reactance versus frequency, we adjusted microstructure layout of the sub-wavelength unit cell until its reflection phase variation become gentle over X and Ku band. Six different scaling unit cells are chosen to form diffuse scattering metasurface. Simulation and experimental results exhibit that monostatic RCS reduction more than 10 dB can be realized over X and Ku band.

INDEX TERMS Broadband, diffuse scattering metasurface, equivalent transmission line model, RCS reduction.

I. INTRODUCTION

Metamaterial is a kind of artificial structure composite or material that exhibits properties not found in natural materials or compounds. Since 3-dimensional metamaterials usually have relatively narrow bandwidth and heavy thickness, their application are limited. Many scholars have tried to broaden their bandwidth and reduce their thickness [1]–[3]. Metasurface with ultrathin thickness is then put forward. Compared to 3-dimensional metamaterial with similar electromagnetic properties, metasurface is flexible, conformal and processing easily [4].

In 2011, F. Capasso use V-shaped antennas as unit cell structures to design phase gradient metasurface and find series of its special optical phenomena such as anomalous reflection and refraction [5]. At same time, generalized reflection and refraction laws are deduced and verified experimentally. The results show that the additional gradient phase shift along propagation path of light can provide great flexibility in molding optical wavefront. It breaks the constraint of standard optical components, which rely on gradual phase accumulation along the optical path to change the wavefront of propagating light [6].

From then on, more researchers focus on anomalous electromagnetic phenomena brought by metasurface and it is applied promptly in various fields, including but not limited to wave-front control technology [7], [8], polarization convertor, propagating waves(PW) to surface waves(SW) convertor [9], [10], ultrathin flat lenses [11], holographic technology, vortex-beam generators. It is also used to reduce monostatic radar cross section (RCS) [12]–[16]. For example, it is demonstrated that metasurfaces can be used to realize specific electromagnetic characters such as reflection in specific direction without altering its physical shape, by utilizing achromatic phase shift stemming from spin-orbit interaction in ultrathin space-variant and spectrally engineered metasurfaces [17]. In [18], an anisotropic metal-mirror, which can accomplish achromatic polarization transformation within 4-octave bandwidth (twice as large as that of previous broadband converters) is presented.

Although metasurface has property controlling electromagnetic waves, narrow bandwidth often limited its

The associate editor coordinating the review of this manuscript and approving it for publication was Muhammad Zubair.

application. From early stage to present, many scholars have been working to broaden its operation bandwidth. The initial metasurface constructed by V-shaped unit cells exhibit abnormal reflection and refraction phenomenon, but its bandwidth is only 1.0-1.9μm [19]. The reflective phase gradient metasurface with anomalous reflection for linearly polarized waves built by Yongfeng Li et al. reaches wider frequency band lately [20]. In 2013, Mingbo Pu et al. propose a metasurface based on subwavelength unit cells with low Q values which exhibit anomalous reflections over 8-12 GHz [21]. An equation calculating reflection phase of the unit cell is also given as follows:

$$\varphi_r = \arg\left(\frac{(1-\sqrt{\epsilon_2}-Y_s/Y_0)-(1+\sqrt{\epsilon_2}-Y_s/Y_0)\exp(2ikh)}{(1+\sqrt{\epsilon_2}-Y_s/Y_0)-(1-\sqrt{\epsilon_2}-Y_s/Y_0)\exp(2ikh)}\right) \tag{1}$$

In [21], bandwidth of the metasurface occurring anomalous reflection is broadened by adding a gradient-index dielectric layer on top surface of the metasurface, which enlarges reflection phase range of unit cells to 0-360°. However, the variation range of reflection phase is not uniform within range of 0-360°.

In this paper, an equivalent transmission line model of the unit cell is developed to deduce reflection phase of the microstructure layer of the unit cells at first. It correlates reflection phase of the unit cell to reactance of the microstructure layer, thickness of the dielectric layer and dielectric permittivity directly. Then the transmission line models of series resonance circuit and shunt resonance circuit are compared. By analyzing the normalized reactance X/Z0 of these two equivalent transmission line models, it is found that the normalized reactance X/Z0 of the parallel resonance circuit model is closer to the expected normalized reactance. Referring to the equivalent transmission line model of shunt resonance circuit, we proposed a subwavelength unit cell. We adjust and optimize structure and size of the unit cell, six unit cells with different physical size are determined ultimately, of which reflection phases can cover entire 0-360° within range of 8.0-17.0 GHz. The phase random metasurfaces is then constructed by these subwavelength unit cells which exhibit diffuse scattering within frequency band of 7.0-16.0 GHz. Compared with that one presented in [21], bandwidth of the metasurface proposed is doubled, and there is no need to add gradient refractive index dielectric layer on top of the metasurface. This unit cell can also be used to compose phase gradient metasurfaces with broadband anomalous reflections.

II. DESIGN OF METASURFACES

A. EQUIVALENT TRANSMISSION LINE MODEL OF TYPICAL SUBWAVELENGTH UNIT CELLS

We develop equivalent transmission line model to analyze reflection phase distribution of the metasurface. At first, the reflection constant of a unit cell is extracted as follows. A typical subwavelength unit cell configuration is as shown in Fig.1(a) which usually has three layers. The upper layer is microstructure layer. The middle is dielectric layer with relative permittivity ε_r and thickness d, and the bottom layer is ground (perfect conductor layer). The microstructure layer can be equivalent to a series resonance circuit or a shunt resonance circuit [20]. The dielectric layer and ground plane can be equivalent to a lossless transmission line with a short-circuited terminal load, of which characteristic impedance is Z_m. Thus, two models for subwavelength unit cells based on equivalent transmission line are gained as Fig.1(b) and Fig.1(c). Fig.1(b) is a series resonance circuit model and Fig.1(c) a shunt resonance circuit model. The correspondence between each part of the subwavelength unit and its equivalent element in models is indicated in Fig.1.

The equivalent lumped element parameters R, L, and C (or R_1, R_2, L_1, L_2, C_1, and C_2) of the structural layers in its equivalent transmission line model depend on its physical size parameters. Its equivalent impedance Z_s in series resonance model and shunt resonance model can be expressed as follows respectively:

$$Z_s = R + j\frac{\omega^2 LC - 1}{\omega C} = R + jX \tag{2}$$

or

$$\begin{aligned} Z_{s1} &= R_1 + j(\omega L_1 + \frac{1}{\omega C_1}) \\ Z_{s2} &= R_2 + j(\omega L_2 + \frac{1}{\omega C_2}) \\ Z_s &= \frac{Z_{s1}Z_{s2}}{Z_{s1}+Z_{s2}} = R + jX \end{aligned} \tag{3}$$

where R is equivalent resistance of the microstructure layer. X is equivalent reactance of the microstructure layer. L is equivalent inductance and C is equivalent capacitor. Since resistance of the micro-structured layer usually is very small in practice, it can be neglected. Then we can use lossless transmission line model to analyze it.

The middle dielectric layer and the conductor ground can be regarded as a lossless transmission line with short circuit terminal of which length is d and characteristic impedance Z_m. Then the input impedance Z_d of this transmission line can be written as:

$$Z_d = jZ_m \tan(\beta_m d) \tag{4}$$

where β_m is propagation constant of electromagnetic wave in the dielectric layer.

Total impedance Z_{total} of the equivalent transmission line model is shunt impendence of the microstructure layer impedance Z_s and the dielectric layer impedance Z_d:

$$Z_{total} = \frac{Z_s Z_d}{Z_s + Z_d} \tag{5}$$

The reflection coefficient Γ at input port of the equivalent transmission line model can be derived by total impedance Z_{total} and characteristic impedance Z_0 of air:

$$\Gamma = \frac{Z_{total} - Z_0}{Z_{total} + Z_0} \tag{6}$$

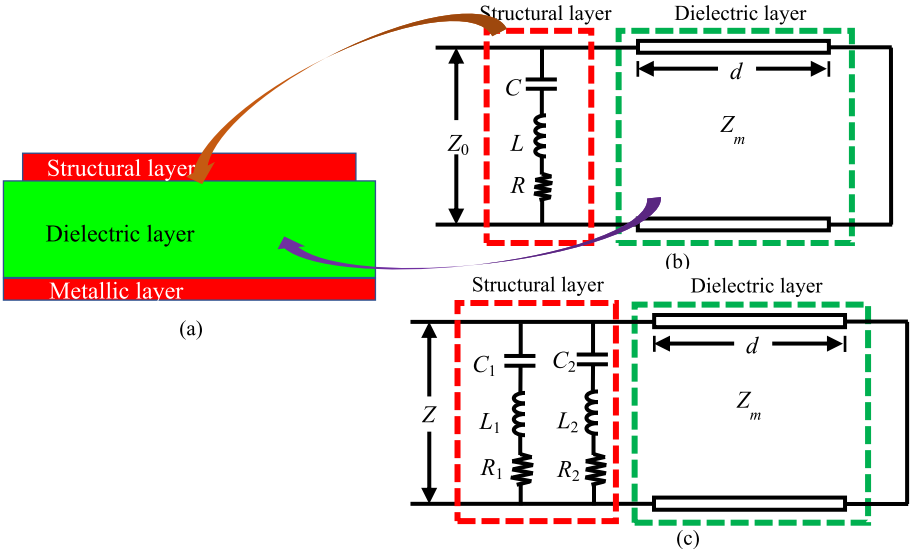

FIGURE 1. Unit cell and equivalent models (a) The equivalent transmission line model of typical subwavelength unit cell. (b) The equivalent series resonance model. (c) The equivalent shunt resonance model.

Then the reflection phase φ at the input port of the transmission line model is:

$$\varphi = \arctan\frac{\mathrm{Im}(\Gamma)}{Re(\Gamma)} = \arctan\left(\frac{2\cdot\frac{X}{Z_0}\cdot\tan(\beta_m d)\cdot\left(\tan(\beta_m d)+\frac{X}{Z_0}\cdot\sqrt{\varepsilon_r}\right)}{\left(\frac{X}{Z_0}\cdot\tan(\beta_m d)\right)^2-\left(\tan(\beta_m d)+\frac{X}{Z_0}\cdot\sqrt{\varepsilon_r}\right)^2}\right) \tag{7}$$

Thus, to design a subwavelength unit cell with a stable phase difference, it is necessary to make the phase difference between two adjacent unit cells have a constant value versus frequency:

$$\varphi_{n+1}(f)-\varphi_n(f)=\Delta \tag{8}$$

φ_{n+1} and φ_n are phases of two adjacent unit cells.

If there is no microstructure layer on top of the dielectric layer, the reflection phase should be sum of phase delay (2βmd) in the dielectric layer and phase change (π) caused by total reflection. We assume the reflection phase in this case as phase reference φ_0:

$$\varphi_0(f)=2\beta_m d+\pi \tag{9}$$

Unit cells with stable phase gradient distributions can be constructed by calculating the phase difference between phase reference φ_0 and reflection phase of subwavelength unit cells with different physical size parameters. A quadratic equation with one unknown X/Z_0 can be gained by combining (7), (8),and (9):

$$a\cdot\left(\frac{X}{Z_0}\right)^2+b\cdot\frac{X}{Z_0}+c=0 \tag{10}$$

where,

$$a=2\sqrt{\varepsilon_r}-\tan(\beta_m d)\cdot\tan(2\cdot\beta_m d+\Delta)+\frac{\tan(2\cdot\beta_m d+\Delta)}{\tan(\beta_m d)}\varepsilon_r$$
$$b=2\tan(\beta_m d)+2\sqrt{\varepsilon_r}\tan(2\cdot\beta_m d+\Delta)$$
$$c=\tan(\beta_m d)\cdot\tan(2\cdot\beta_m d+\Delta)$$

Let $\Delta=\pi$ in (10), an curve of ideal normalized reactance X/Z_0 versus frequency can be gained as shown by the red line in Fig.2(a). As is illustrated, the expected normalized reactance X/Z_0 versus frequency curve shows a nonlinear relationship, and there are sharp jigs at some frequency points. In order to compare relationship of practical normalized reactance X/Z_0 of series resonance model and that of shunt resonance model to the ideal normalized reactance, we choose a typical set of value as example.

Firstly, according to the reflection phase shift chosen for each subwavelength unit cell, S11 of the unit cell can be determined. Then, we construct series resonance model composed of one inductance and one capacitance as well as shunt resonance model consists of two series resonance branches respectively. Finally, the inductance and the capacitance values can be derived as follows by assuming S_{11} of these two types of model equal to S_{11} of the unit cell.

The first set of value corresponds to the series resonance model. The capacitance and inductance values are L=13730pH and C=20fF respectively. The normalized reactance X/Z_0 can be calculated by $X/Z_0 = (\omega L-1/\omega C)/Z_0$ and is denoted in blue dashed line in Fig.2(a). As is shown in Fig.2(b)(enlarged Fig.2(a)), the normalized reactance curve of series resonance model coincides with the expected normalized reactance curve over frequency bandwidth of 8.8-11.6 GHz.

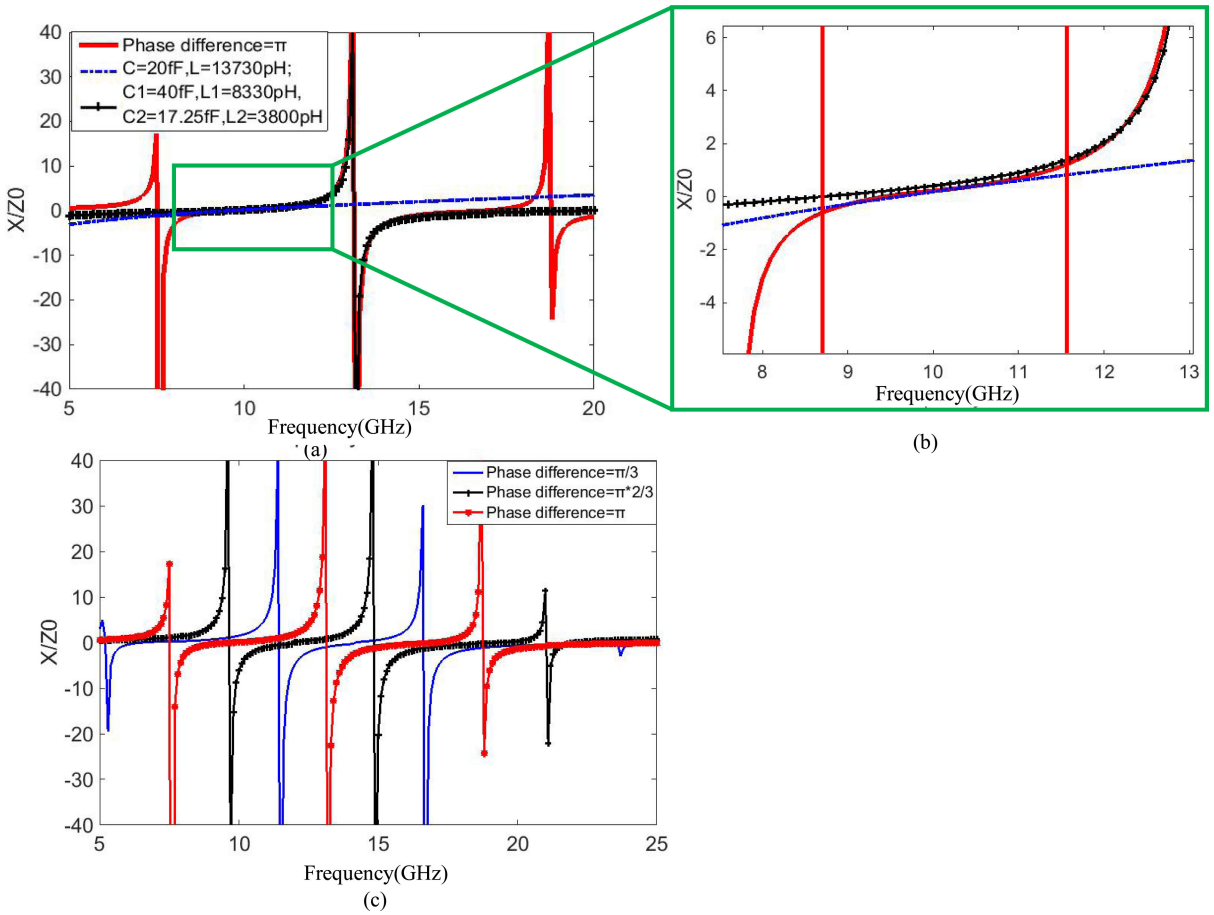

FIGURE 2. Normalized reactance versus frequency (a) the expected normalized reactance X/Z_0 under $\Delta = \pi$ and actual normalized reactance X/Z_0 of two equivalent transmission line models. (b) the enlarged view of region inside green rectangle box in Fig.2(a). (c) the expected normalized reactance X/Z_0 curve under $\Delta = \pi/3$, $\Delta = 2\pi/3$ and $\Delta = \pi$ respectively.

The second set of value corresponds to the shunt resonance model. The inductance and capacitance values of two series resonance branches are $C_1 = 40$fF, $L_1 = 8330$pH, $C_2 = 17.25$fF, $L_2 = 3800$pH. The normalized reactance X/Z_0 versus frequency curve is denoted by black "+" line in Fig.2(a). As is shown in Fig.2(a), the normalized reactance X/Z_0 curve of shunt resonance model coincides with the expected normalized reactance curve over frequency range of 8.8-17.5GHz.

Thus, reflection phase of the equivalent transmission line model of shunt resonance circuit can reach phase difference of 180° referring to $\varphi_0(f)$ over frequency bandwidth 8.8-17.5GHz, Whereas reflection phase of the equivalent transmission line model of series resonance can cover phase difference of 180° only within frequency range of 8.8-11.6 GHz referring to $\varphi_0(f)$. Phase difference of the equivalent transmission line model of shunt resonance can be stable between two resonance points of two series branches which are 8.72GHz and 19.7GHz respectively.

To verify above conclusion further, the expected normalized reactance X/Z_0 versus frequency curves under $\Delta = \pi/3$ and $\Delta = 2\pi/3$ are deduced as well, as shown by blue solid line and black "+" line in Fig. 2(c) respectively. As is shown in Fig.2(c), two expected normalized reactance curves of $\Delta = \pi/3$ and $\Delta = 2\pi/3$ are uniform between two jump points. It proves that phase difference between two adjacent jumping points is π and phase difference between a jumping point and the jumping point after the next is 2π.

B. SUBWAVELENGTH UNIT CELLS BASED ON SHUNT RESONANCE MODEL

Based on analysis in Section A, there is a stable phase difference over a wider frequency range with shunt resonance equivalent model. In this section, we design a subwavelength unit cell with shunt resonance feature based on equivalent transmission line model. First, the classic cross-shaped unit cell is chosen. Then we slit the metal arms of it to lead in capacitance effect. Thus, the structure equivalent to series resonance model is built. We further extend length of the cross-shaped horizontal arms and vertical arms at their ends to form another series resonant branch. Till now, the unit cell equivalent to shunt resonance circuit is developed as shown in Fig.3(b). According to previous conclusion drawn from comparison between series resonance circuit and parallel resonance circuit. Operation bandwidth of the classic cross-shaped unit cell is broadened. The unit cell developed

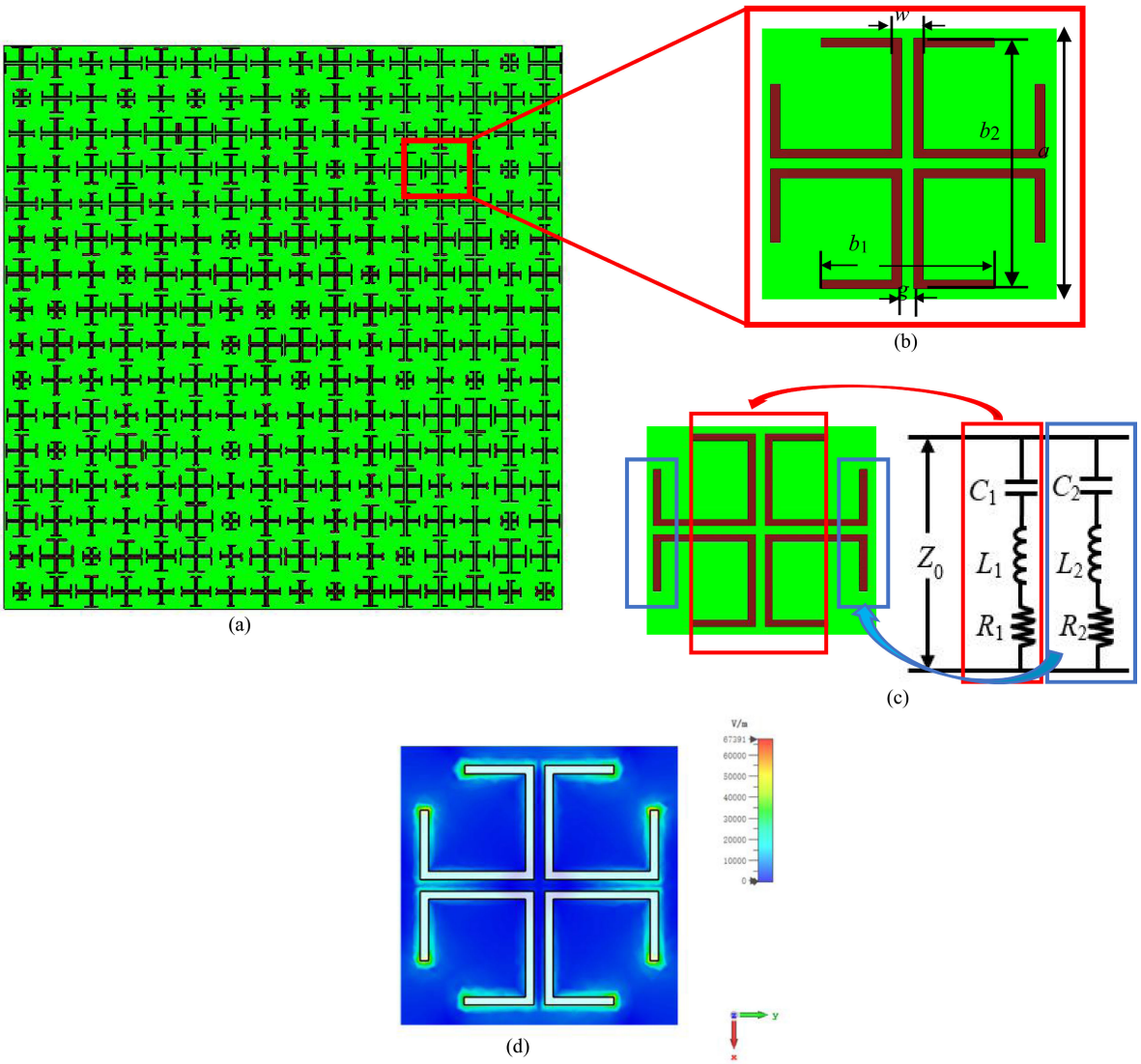

FIGURE 3. **Metasurface (a) diffuse scattering metasurface constructed by subwavelength units. (b) subwavelength unit with shunt resonance feature. (c) the subwavelength unit cell and its corresponding shunt resonance transmission line model. (d) corresponding electric field distribution on this subwavelength unit.**

consists of three layers. The upper layer is a microstructure layer with shunt resonance feature. The middle layer is a dielectric layer with $\varepsilon r = 2.65$ and $d = 3.5$ mm, and the bottom layer is a metal ground plane. The thickness of upper and bottom metal layer is t1. After optimizing, we determine that size of the unit cell is a=10mm. Four parameters g, b_1, b_2, and w of surface microstructure are denoted in Fig.3(b) correspondingly. Since g is given, the equivalent impedance Z_s of the microstructure layer is adjusted by the other three parameters. Fig.3(c) shows the subwavelength unit cell and its corresponding shunt resonance transmission line model. The region inside the red box of the unit cell in x-axis direction is equivalent to $R_1L_1C_1$ branch and the end-line regions inside two blue boxes of the unit cell in x-axis direction are equivalent to $R_2L_2C_2$ branch. Corresponding electric field distribution on this subwavelength unit is presented in Fig.3(d)

Since equivalent capacitance and inductance values of the microstructure layer changes with physical size parameters of the unit cell, thereby, equivalent impedance of the microstructure layer changes. Equivalent impedance of the microstructure layer directly affects reflection phase variation of the subwavelength unit cells. We optimize b_1, b_2, and w of this unit cell configuration at first. Based on final optimization results, six subwavelength unit cells of different physical sizes which show the best reflection phase distribution with phase difference of 60° are determined. The values of b_1, b_2, and w for these six subwavelength unit cells are listed in Table 1. To compare actual normalized reactance X/Z_0 curve of six units developed to the expected normalized reactance X/Z_0 curve, we calculate capacitance and inductance values of each unit cell by S-parameter inversion. Since the subwavelength unit cells presented feature shunt resonance favors, C_1, L_1, C_2, and L_2 corresponding to six

TABLE 1. Physical parameters for six subwavelength unit cells and their corresponding capacitance and inductance values.

Unit Cell	Size Parameters (mm)			L and C Values			
	B1	B2	W	C_1(fF)	L_1(pH)	C_2(fF)	L_2(pH)
1	2.2	6.0	0.8	7.54	14015	3.35	9015.03
2	3.0	7.5	1.5	10.0	2850.06	18.87	8050
3	3.6	8.1	1.4	9.5	5350.06	22.7	7740
4	4.2	8.4	1.0	11	4745.06	24.75	10165
5	5.4	8.6	1.0	16.21	3605	30.07	10500
6	6.4	9.0	1.0	21.67	3300	36.5	11400

subwavelength unit cells can be derived as shown in Table 1. We simulate $|S_{11}|$ of the unit cells and the results closes to 0dB within operation frequency band. It means the resistance R_1 and R_2 are relatively small and can be neglected.

Six reflection phases versus frequency curves corresponding to six subwavelength unit cells with different physical size parameters are illustrated in Fig.4(a). As is shown in Fig.4(a), reflection phases of the six unit cells vary with frequency linearly within frequency bandwidth 8.0-16.0GHz. Considering the phase difference between two first cells of adjacent lattices (six unit cells with different physical size parameters consist of a lattice under periodic layout) should be 360°, we think reflection phase variation range of each unit cell covers 0-300°. Phase difference between adjacent unit cells keeps 60° approximately over entire range of 8.0-16.0GHz.

Fig.4(b) compares actual normalized reactance X/Z_0 curve of the third largest and the smallest unit cell with the expected normalized reactance X/Z_0 curve as $\Delta = \pi/3$ where X/Z_0 are calculated using corresponding L and C values listed in Table 1. The blue "$*$" line is normalized reactance X/Z_0 curve of the third largest unit cell and the black "$+$" line is that of the smallest unit cell. The actual normalized reactance curves of these two unit cells both agree very well with the expected one. Besides, the jumping points of these two curves also in agreement with the two jumping points of the expected normalized reactance curve. It indicates that the phase difference between these two unit cells is π. This is verified in Fig.4(a). Similarly, actual normalized reactance X/Z_0 curves of the largest unit cell and the fourth largest one is compared with the expected normalized reactance X/Z_0 curve as $\Delta = 2\pi/3$ in Fig.4(c). The phase difference between these two unit cells is also π as is shown. Further, Fig.4(d) shows the actual normalized reactance X/Z_0 curves of the second largest unit cell and the fifth largest one and the expected normalized reactance X/Z_0 curve when $\Delta = \pi$. The phase difference between these two unit cells proves π as well. Above all, the reflection phase difference between adjacent unit cells is $\pi/3$.

C. EQUIVALENT TRANSMISSION LINE MODEL OF TYPICAL SUBWAVELENGTH UNIT CELLS

There are several ways to reduce RCS. In "Radar Cross Section Manual" [22] Ruck classifies them into:

1. Absorbing material. Absorbing materials can absorb electro-magnetic energy and convert it into heat energy or other forms of energy so that scattering energy is low.

2. Low scattering microstructure/material. Low scattering structure/material does not absorb electromagnetic energy but change direction of reflection or transmission waves so that electromagnetic energy received at the receiver is low.

3. Low scattering shape. It can also change the path of incident waves so that energy returning to receiver as low as possible.

It is the second way above utilizing random phase metasurface to reduce RCS. We construct rough surface composed of unit cells designed specifically for microwave wavelength. Because diffuse scattering convey energy evenly, RCS selected by receiver is low. Surface roughness depends on wavelength and angle of incident wave. As shown in Fig.5, when the surface is perfectly smooth, two reflection beams are parallel and have the same phase, which is called specular reflection. When the surface is rough, two reflection waves are no longer in the same phase. The phase difference can be expressed as:

$$\Delta\varphi = 2kd\cos\theta_i \tag{11}$$

If the phase difference between two reflection waves is much less than $\pi/2$, the surface closes to a smooth plane feature. When the phase difference becomes relatively large, the specular reflection weakens due to interference effect of reflection waves of different points and more electromagnetic energy is scattered to other direction. Fraunhofer [23] points out that a surface can be regarded as the rough surface if only $d > \lambda/(32\cos\theta_i)$ (which can be expressed as phase difference $\Delta\varphi > 2\pi/(16\cos\theta i)$, i.e. phase difference $\Delta\varphi > \pi/8$ when incident angle $\theta_i = 0$) within microwave band. Otherwise, it is smooth surface. For a smooth surface, specular reflection dominates. As the surface becomes rougher, specular reflection degenerates and much more energy is scattered to other direction. Diffuse scattering dominates then.

Based on principle above, we construct phase random metasurface using the unit cells presented which show required reflection phases over relatively broad bandwidth. The metasurface developed demonstrates diffuse scattering feature within 6.8GHz-16.4GHz.

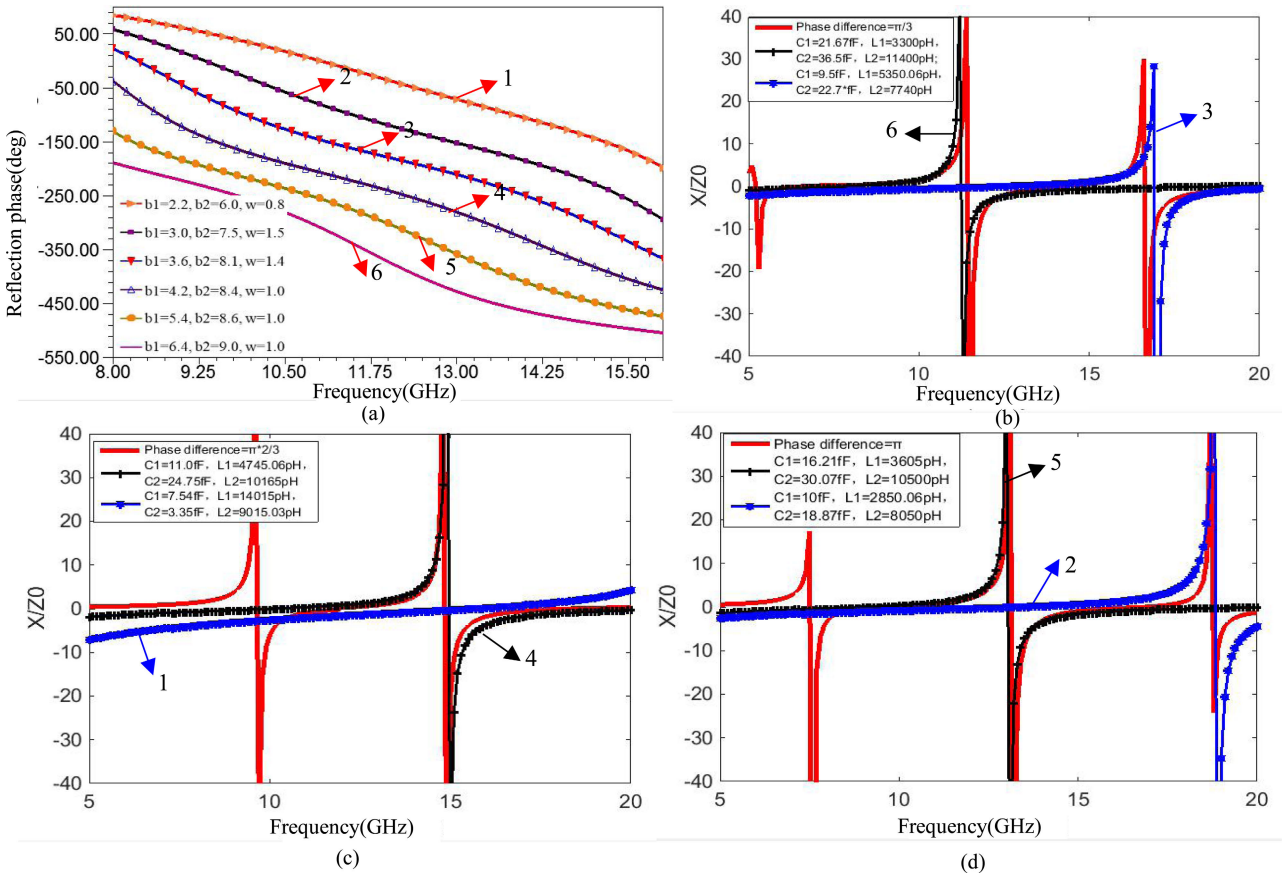

FIGURE 4. Reflection phase and normalized reactance (a) variation of the reflection phase of six subwavelength unit cells with different physical sizes versus frequency. (b) actual normalized reactance X/Z_0 curves for the 3rd largest and the smallest unit cells and expected normalized reactance X/Z_0 curve as $\Delta = \pi/3$. (c) actual normalized reactance X/Z_0 curves for the largest and the fourth largest unit cells and the idealized normalized reactance X/Z_0 curve as $\Delta = 2\pi/3$. (d) actual normalized reactance X/Z_0 curve for the second and the fifth largest unit cells and the idealized normalized reactance X/Z_0 curve for $\Delta = \pi$.

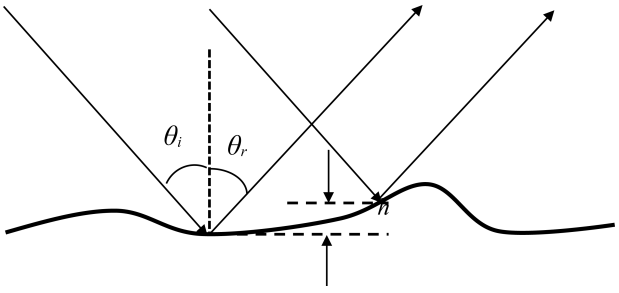

FIGURE 5. Fraunhofer criterion on surface roughness.

Since phase range is 2π, $\pi/3$ is chosen as phase gradient between adjacent unit cells and six types of unit cells with different sizes of which reflection phase are analyzed in above section are used.

The random phase metasurface is as shown in Fig.3(a). It consists of 16×16 unit cells. Its size is 160mm $\times$ 160mm.

In order to verify its diffuse scattering characteristics, we calculate RCS of the metasurface under TE and TM incident wave receptively. Monostatic RCS versus frequency curves under normal TE and TM incident wave are shown in Fig.6(a) where the red "+" line is for TE incident wave and the blue "Δ" line is for normal TM incident wave. Black solid line is monostatic RCS of a metal plate of the same size with the metasurface presented. As is illustrated in Fig.6(a), monostatic RCS variations with frequency of the metasurface developed under TE and TM incident wave are similar to each other. Compared to monostatic RCS of the metal plate of the same size, they both reach more than 10dB RCS reduction frequency range of 6.8 to 16.4 GHz. Due to symmetric configuration of the unit cells, scattering characteristics of the metasurface is insensitive to polarization feature of incident wave.

In order to observe diffuse scattering phenomenon occurring on the metasurface visually, we simulate three-dimensional farfield pattern at following four frequency points 7.0GHz, 10.0GHz, 13.0GHz, and 16.0GHz respectively. Fig.6(c) is the pattern under normal TE incident wave. Diffuse scattering effects become stronger as frequency increases which coincides with general principle on rough surface scattering. Besides, bistatic RCS of the metasurface under normal TE incident wave is also calculated and compared to that of metal plate of the same size at 13.0 GHz. The results are shown in Fig.6(d). Except that RCS of the metasurface at bistatic angle Theta=0° (corresponding to monostatic RCS)is lower than that of the metal plate significantly,

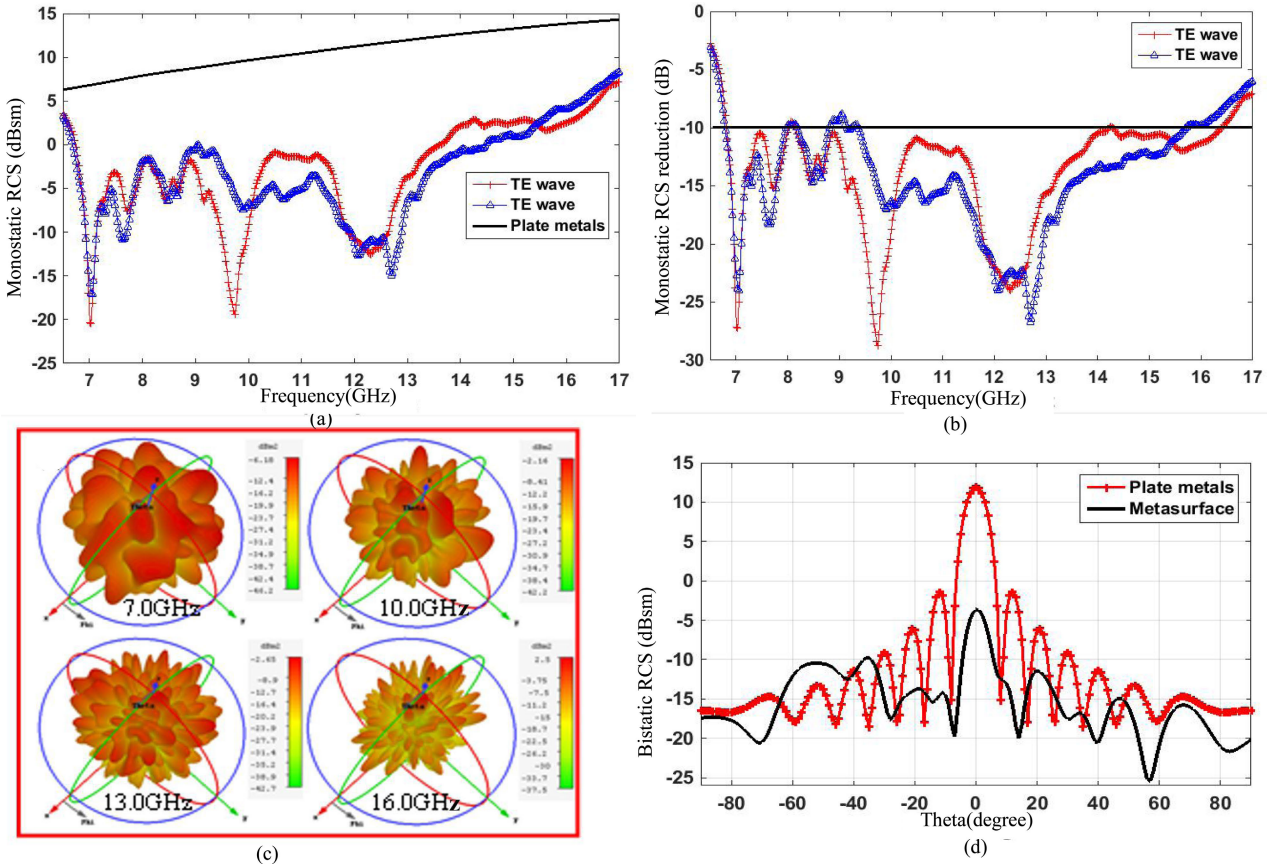

FIGURE 6. RCS of metasurface (a) monostatic RCS of the metasurface under normal TE and TM incident wave and that of metal plate of the same size. (b) monostatic RCS reduction of the metasurface compared to the metal plate. (c) Three-dimensional farfield scattering patterns of the metasurface at 7.0GHz, 10.0GHz, 13.0GHz, and 16.0GHz. (d) Comparison of bistatic RCS of the metasurface to that of the same-size metal plate at 13.0 GHz (yoz plane).

RCS reduction at other bistatic angles become less due to low bistatic RCS of the metal plate itself under normal incidence. It also proves true that diffuse scattering energy is distributed evenly where spectrum reflection concentrates energy to definite direction

We also study scattering properties of the metasurface presented under oblique incident conditions. Setting incident angles as 15°, 30°, and 45° respectively, bistatic RCS at specular reflection angle direction (i.e. incident angle θi is equal to reflection angle θr) are calculated and results are denoted in Fig.7 by different colors. As is shown in the diagram, compared to bistatic RCS of smooth metal plate under corresponding incident angle 15°, 30°, RCS reduction caused by the metasurface can reach more than 10dB over bandwidth 6.4GHz-16.4GHz. In Fig.7(b) which compares RCS reduction between the metasurface and the smooth metal plate in detail further, it can be found that RCS reduction under incident angle 45° is approximately 7.5dB over most range of 6.4 GHz-16.4GHz, since RCS of the smooth metal plate decreases too. In other words, when incident angle reaches as large as 45°, RCS reduction effect of the metasurface presented degenerates. The phase random metasurface developed can realize effective RCS reduction under incident angle less than 45° over X and Ku bands.

There are two factors to cause little degeneracy of RCS reduction under large incident angle. The electromagnetic response to radiation of the metasurface unit cell changes with incident angle variation. When the incident direction is perpendicular to the metasurface, magnetic response of the unit cell is mainly generated by the gap between the parallel patch lines. When incident angle changes, the orientation of magnetic field changes. Under excitation of magnetic field component perpendicular to the metasurface, the gap between the patch rings also constitutes a capacitive effect. Thus, the electromagnetic response of each unit cell will change. Ultimately, the resonance characteristics and phase versus frequency curve are affected. In addition, as incident angle changes, the difference of incident phase on unit cells also changes. Then, the phase difference of the reflection wave of unit cells also changes which results in variation of RCS reduction effects.

To verify above simulation results, the proposed metasurface of 160mm×160mm composed of 16 × 16 unit cells is fabricated. Monostatic RCS of the random phase metasurface is tested in anechoic chamber under normal TE and TM incident wave respectively. Agilent N5230C vector network analyzer is used and two dual-ridged pyramidal horns with standard gain, of which frequency bandwidth is 9-16GHz,

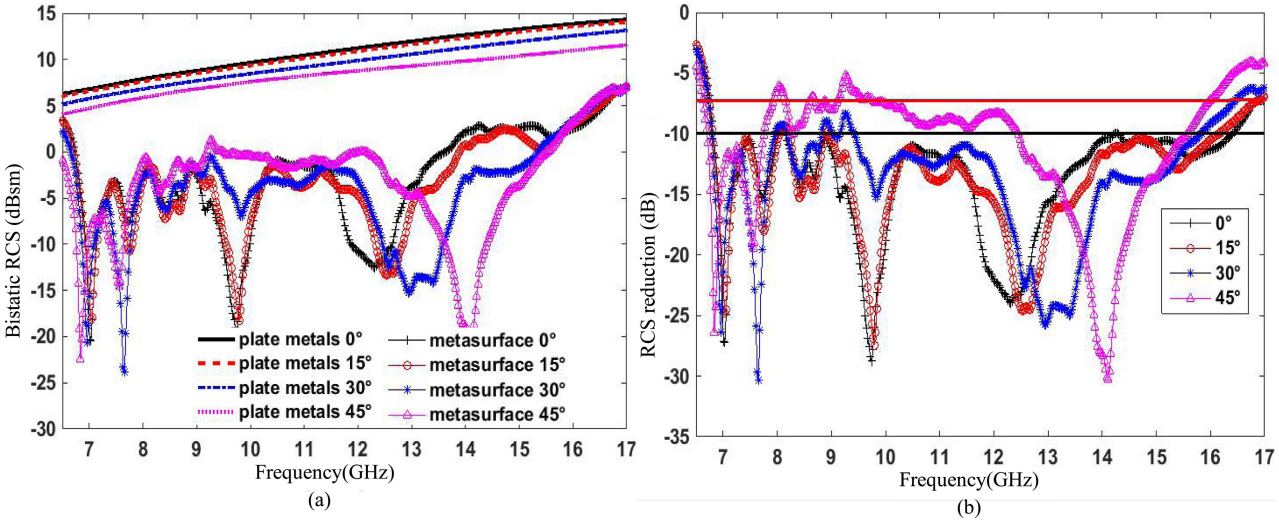

FIGURE 7. Bistatic RCS of metasurface (a) bistatic RCS of the metasurface and smooth metal plate at specular reflection angles 0°, 15°, 30°, and 45°. (b) RCS reduction of metasurface with respect to smooth metal plate under incident angles 0°, 15°, 30°, and 45°.

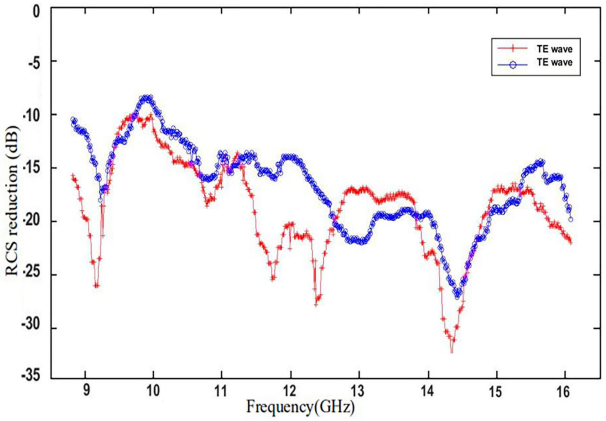

FIGURE 8. Test RCS results of the metasurface and smooth metal plate of the same size.

are used as transmission and reception antennas. To eliminate the interference of environment, time-domain gating in the network analyzer is adopted in experiments. Fig.8 shows the measured results. As is shown in above diagram, monostatic RCS reduction exceeds 10 dB over 9-16GHz in two incident cases which agrees with simulation results considering fabrication and measurement errors. the measured results verify the low scattering of this novel design.

III. CONCLUSION

In this paper, equivalent transmission line model is used to analyze reflection phase feature of the metasurface unit cell. According to analysis based on the model, a subwavelength unit cell with equivalent shunt resonance model has stable reflection phase over wider frequency bandwidth than one with equivalent series resonance model. Then, a unit cell configuration exhibiting stable reflection phase over 6.8-16.4GHz is presented. According to Fraunhofer criterion on diffuse scattering, six optimized unit cells with different physical sizes and equal phase gradient are determined to construct the metasurface with random phase distribution. The metasurface presented exhibits expected diffuse scattering characteristics over 6.8-16.4GHz. Thus, monostatic RCS reduction can reach more than 10dB under both normal TE and TM incidence. When the incident angle is less than 45°, effective RCS reduction can also be realized over the corresponding band. The way to design is applicable to metasurfaces with wideband characteristics.

REFERENCES

[1] D. R. Smith, "Metamaterials and negative refractive index," *Science*, vol. 305, no. 5685, pp. 788–792, Aug. 2004.

[2] R. W. Ziolkowski and E. Heyman, "Wave propagation in media having negative permittivity and permeability," *Phys. Rev. E, Stat. Phys. Plasmas Fluids Relat. Interdiscip. Top.*, vol. 64, no. 5, Oct. 2001, Art. no. 056625.

[3] H. Cory and C. Zach, "Wave propagation in metamaterial multi-layered structures," *Microw. Opt. Technol. Lett.*, vol. 40, no. 6, pp. 460–465, Mar. 2004.

[4] M. Pu, P. Chen, C. Wang, Y. Wang, Z. Zhao, C. Hu, C. Huang, and X. Luo, "Broadband anomalous reflection based on gradient low-Q meta-surface," *Aip Adv.*, vol. 3, no. 5, May 2013, Art. no. 052136.

[5] N. Yu, P. Genevet, M. A. Kats, F. Aieta, J.-P. Tetienne, F. Capasso, and Z. Gaburro, "Light propagation with phase discontinuities: Generalized laws of reflection and refraction," *Science*, vol. 334, no. 6054, pp. 333–337, Oct. 2011.

[6] S. Sun, K.-Y. Yang, C.-M. Wang, T.-K. Juan, W. T. Chen, C. Y. Liao, Q. He, S. Xiao, W.-T. Kung, G.-Y. Guo, L. Zhou, and D. P. Tsai, "High-efficiency broadband anomalous reflection by gradient meta-surfaces," *Nano Lett.*, vol. 12, no. 12, pp. 6223–6229, Dec. 2012.

[7] H. Shi, J. Li, A. Zhang, Y. Jiang, J. Wang, Z. Xu, and S. Xia, "Gradient metasurface with both polarization-controlled directional surface wave coupling and anomalous reflection," *IEEE Antennas Wireless Propag. Lett.*, vol. 14, pp. 104–107, 2015.

[8] Y. Li, J. Zhang, S. Qu, J. Wang, H. Chen, L. Zheng, Z. Xu, and A. Zhang, "Achieving wideband polarization-independent anomalous reflection for linearly polarized waves with dispersionless phase gradient metasurfaces," *J. Phys. D, Appl. Phys.*, vol. 47, no. 42, Oct. 2014, Art. no. 425103.

[9] S. Sun, Q. He, S. Xiao, Q. Xu, X. Li, and L. Zhou, "Gradient-index meta-surfaces as a bridge linking propagating waves and surface waves," *Nature Mater.*, vol. 11, no. 5, pp. 426–431, May 2012.

[10] F. Aieta, P. Genevet, M. A. Kats, N. Yu, R. Blanchard, Z. Gaburro, and F. Capasso, "Aberration-free ultrathin flat lenses and axicons at telecom wavelengths based on plasmonic metasurfaces," *Nano Lett.*, vol. 12, no. 9, pp. 4932–4936, Sep. 2012.

[11] Y. Zhang, L. Liang, J. Yang, Y. Feng, B. Zhu, J. Zhao, T. Jiang, B. Jin, and W. Liu, "Broadband diffuse terahertz wave scattering by flexible metasurface with randomized phase distribution," *Sci. Rep.*, vol. 6, no. 1, May 2016, Art. no. 26875.
[12] K. Chen, Y. Feng, Z. Yang, L. Cui, J. Zhao, B. Zhu, and T. Jiang, "Geometric phase coded metasurface: From polarization dependent directive electromagnetic wave scattering to diffusion-like scattering," *Sci. Rep.*, vol. 6, no. 1, Oct. 2016, Art. no. 35968.
[13] J. Su, Y. Lu, H. Zhang, Z. Li, Y. Yang, Y. Che, and K. Qi, "Ultra-wideband, wide angle and polarization-insensitive specular reflection reduction by metasurface based on parameter-adjustable meta-atoms," *Sci. Rep.*, vol. 7, no. 1, Feb. 2017, Art. no. 42283.
[14] H. Sun, C. Gu, X. Chen, Z. Li, L. Liu, B. Xu, and Z. Zhou, "Broadband and broad-angle polarization-independent metasurface for radar cross section reduction," *Sci. Rep.*, vol. 7, no. 1, Feb. 2017, Art. no. 40782.
[15] C. L. Holloway, E. F. Kuester, J. A. Gordon, J. O'Hara, J. Booth, and D. R. Smith, "An overview of the theory and applications of metasurfaces: The two-dimensional equivalents of metamaterials," *IEEE Antennas Propag. Mag.*, vol. 54, no. 2, pp. 10–35, Apr. 2012.
[16] Y. Chai, H. Deng, and Q. Xiong, "A dynamically phase tunable metasurface for a broad bandwidth ultra-low radar cross section," *IEEE Access*, vol. 8, pp. 53006–53017, 2020.
[17] M. Pu, Z. Zhao, Y. Wang, X. Li, X. Ma, C. Hu, C. Wang, C. Huang, and X. Luo, "Spatially and spectrally engineered spin-orbit interaction for achromatic virtual shaping," *Sci. Rep.*, vol. 5, no. 1, Sep. 2015, Art. no. 9822.
[18] Y. Guo, Y. Wang, M. Pu, Z. Zhao, X. Wu, X. Ma, C. Wang, L. Yan, and X. Luo, "Dispersion management of anisotropic metamirror for super-octave bandwidth polarization conversion," *Sci. Rep.*, vol. 5, no. 1, Feb. 2015, Art. no. 8434.
[19] X. Ni, N. K. Emani, A. V. Kildishev, A. Boltasseva, and V. M. Shalaev, "Broadband light bending with plasmonic nanoantennas," *Science*, vol. 335, no. 6067, p. 427, Jan. 2012.
[20] Q. Y. Wen, Y. S. Xie, H. W. Zhang, Q. H. Yang, Y. X. Li, and Y. L. Liu, "Transmission line model and fields analysis of metamaterial absorber in the terahertz band," *Opt. Exp.*, vol. 17, no. 22, pp. 20256–20265, Oct. 2009.
[21] F. Costa, A. Monorchio, and G. Manara, "Analysis and design of ultra thin electromagnetic absorbers comprising resistively loaded high impedance surfaces," *IEEE Trans. Antennas Propag.*, vol. 58, no. 5, pp. 1551–1558, May 2010.
[22] X. Luo, "Principles of electromagnetic waves in metasurfaces," *Sci. China Phys., Mech. Astron.*, vol. 58, no. 9, Sep. 2015, Art. no. 594201.
[23] N. Pinel, C. Bourlier, and J. Saillard, "Degree of roughness of rough layers: Extensions of the Rayleigh roughness criterion and some applications," *Prog. Electromagn. Res. B*, vol. 19, pp. 41–63, Jan. 2010.

ZHAOBIN CHEN was born in Shandong, China, in 1990. He received the B.S. degree in electronic information engineering from Shandong Normal University, Shandong, in 2014, and the M.S. degree in electronics and communications engineering from Beihang University, Beijing, in 2018. His research interests include metamaterials, metasurfaces, RF circuit, and plasma.

HUI DENG received the B.S. degree from Xi'an Jiaotong University and the Ph.D. degree from Tsinghua University, Beijing, China, in 1999. From 1999 to 2001, she was a Research Assistant with the State Key Laboratory on Acoustic Field and Acoustic Information, Institute of Acoustics, Chinese Academy of Sciences. Since 2002, she has been an Associate Professor with the School of Electronics and Information Engineering, Beihang University. Her research interests include electromagnetic and acoustic scattering, metamaterials, and applications.

LI ZHENG received the master's degree from the Beijing Electro-mechanical Engineering Institute, Beijing, China, in 2007. He is currently a Senior Engineer with the Beijing Electro-mechanical Engineering Institute. His research interests include electromagnetic scattering calculation and measurement.